

Molecular Cell, Volume 74

Supplemental Information

Distinct USP25 and USP28 Oligomerization States

Regulate Deubiquitinating Activity

Malte Gersch, Jane L. Wagstaff, Angela V. Toms, Bradford Graves, Stefan M.V. Freund, and David Komander

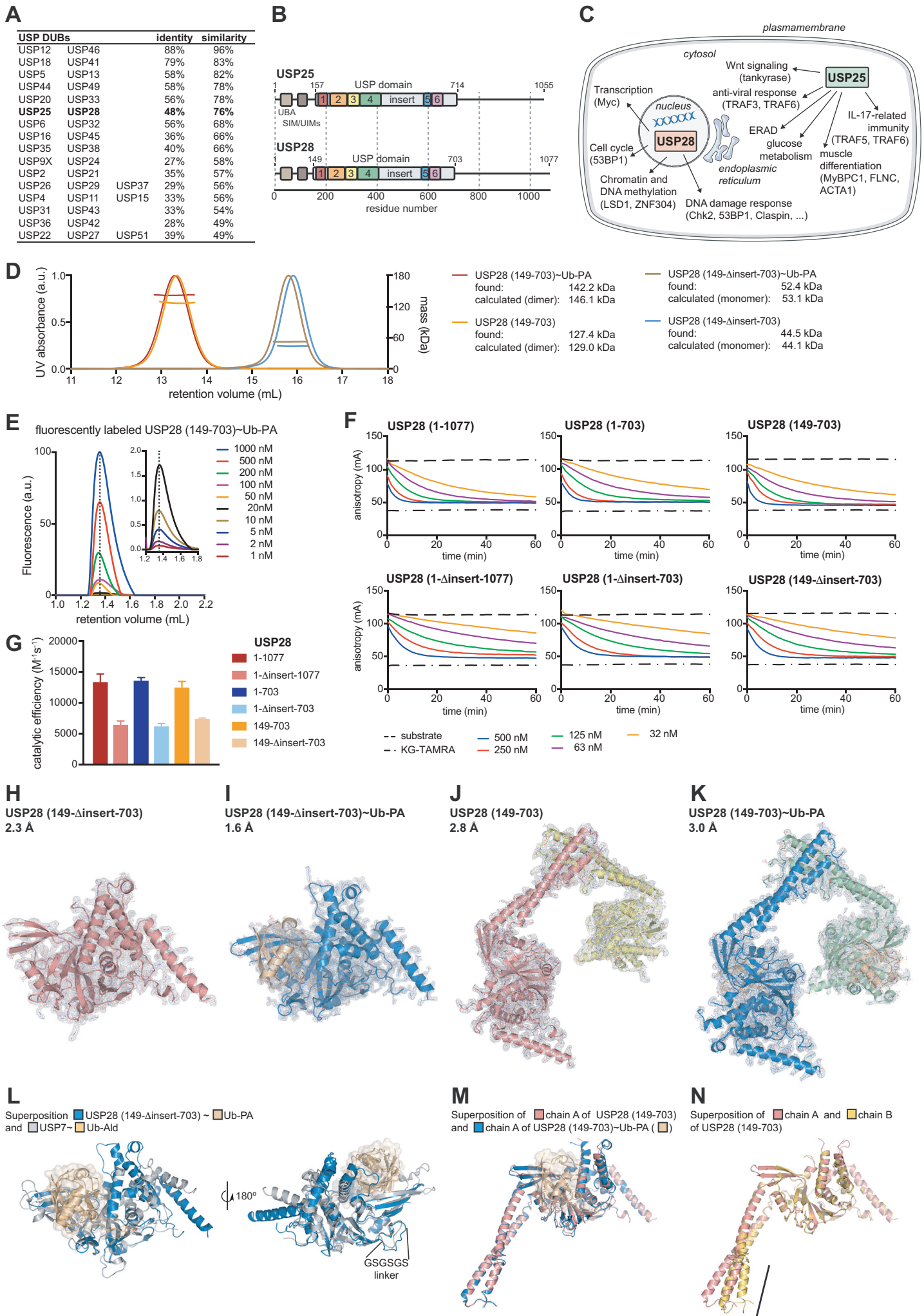


Figure S1. Cellular roles for USP25 and USP28. Biochemical and structural analysis of human USP28 proteins. Related to Figure 1.

(A) List of pairs or triplets of highly homologous human USPs DUBs. The percentage of identical residues as well as identical and similar residues is given. Data are based on alignments of full length protein sequences carried out with the Uniprot webserver. USP25 and USP28 are highlighted in bold.

(B) Schematic representation of human USP25 and USP28 constructs. The catalytic domain is shown in grey, an N-terminal UBA domain, SUMO-interaction motif (SIM) and ubiquitin-interaction motifs (UIMs) are shown in brown. Colored boxes indicate the conserved boxes characteristic of USP domains (Ye et al., 2009).

(C) Previously identified cellular roles linked to USP25 and USP28 indicated by arrows. Subcellular compartments and structures labeled in italics.

(D) SEC-MALS analysis of indicated constructs either in the apo form or bound to Ub-PA. Data of samples in the apo form are as shown in Figure 1C for easy comparison. Identified masses are matched to either monomeric or dimeric expected masses.

(E) A dilution series of a fluorescently labeled USP28 (149-703)~Ub-PA protein sample was analyzed on a size-exclusion chromatography system fitted with a fluorescence detector. Data collected on a more sensitive detector setting are shown as an inset figure. The same central peak position is indicated with dotted lines in both graphs. The given concentrations correspond to the injected sample concentrations.

(F) Representative fluorescence anisotropy-time traces of Ub-KG-TAMRA cleavage assays from averaged technical triplicates of indicated USP28 constructs and concentrations.

(G) Catalytic activities of USP28 constructs determined from data shown in F. Data are shown as mean \pm standard deviation from 2-5 independent experiments, each collected from technical triplicates.

(H, I, J and K) Overall views of the asymmetric units of indicated crystal structures (see Figure 1D-G for cartoon representations). Residues are shown as lines and in cartoon representation. Overlaid electron density maps in grey correspond to weighted $2|F_o|-|F_c|$ electron density contoured at 1σ .

(L) Superposition of the Ub-PA-bound structure of USP28 (149- Δ insert-703) and USP7 bound to ubiquitin-aldehyde (PDB-ID: 1NBF).

(M) Superposition of the apo and Ub-PA-bound structures of USP28 (149-703).

(N) Superposition of the two chains forming the asymmetric unit of the apo structure of USP28 (149-703). Notable differences in the insertion sequence are highlighted with a black line.

Figure S2. Structural analysis of the USP28 insertion sequences. Related to Figure 2.

(A) Pair-wise distance distribution functions $P(r)$ calculated from SAXS data shown in Figure 2A for indicated constructs. The most frequent distances are highlighted with dashed lines and labeled r_1 and r_2 . These are similar to the radius of gyration of the isolated USP domain (r_1) as well as the distance between the two USP domains in the dimer (r_2).

(B) Sequence conservation calculated from 96 USP28 protein sequences annotated as USP28 in the Uniprot database mapped as colored surface on chain A of the USP28 (149-703) structure. Chain B as well as the position of Ub-PA of the USP28 (149- Δ insert-703)~Ub-PA complex structure are shown as semi-transparent cartoons.

(C) Sequence alignment of representative USP28 members of vertebrate families for the insertion sequence. Secondary structure and disorder assignments were carried out with respect to the USP28 (149-703) structure.

(D) Helical wheel diagrams for the three helices $\alpha 1'$, $\alpha 2'$ and $\alpha 3'$ of the USP28 insertion generated with the NetWheels webserver. Residues are colored according to their chemical nature as indicated. Interfaces are labeled and highlighted with black arcs. Cartoon representation of the respective helices as shown in Figure 2C.

(E) SEC-MALS analysis of USP28 catalytic domain constructs where the disordered part of the insertion is deleted (149- Δ (459-528)-703).

(F) Representative fluorescence anisotropy-time traces of Ub-KG-TAMRA cleavage assays from averaged technical triplicates of indicated USP28 constructs and concentrations. Catalytic efficiencies are reported in Figure 2E.

(G) Cartoon representation of inactive USP30 bound to K6-linked diUb (PDB-ID: 5OHP), with distal and proximal ubiquitin moieties labeled and also shown as transparent surfaces (*top left*). Cartoon representation of USP28 (149-703) (*top right*). Superposition of two copies of the USP30 complex on each of the catalytic domains of USP28 (*bottom*).

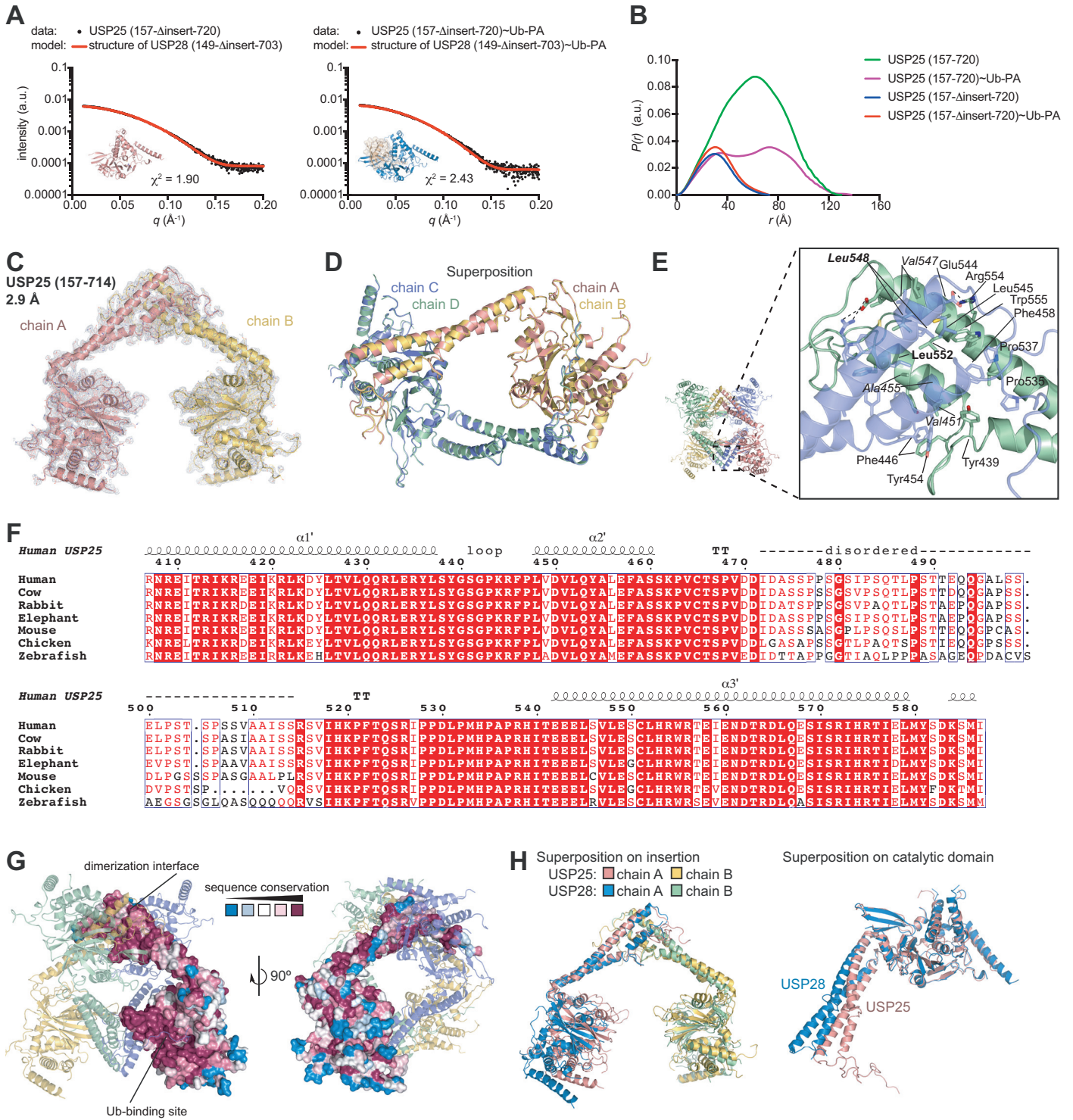


Figure S3. Structural and biochemical analysis of the catalytic domain of USP25. Related to Figure 3.

(A) Small angle X-ray scattering (SAXS) data shown as black dots which was collected from indicated USP25 protein samples. Expected scattering curves are shown in red that were calculated from solved USP28 X-ray crystal structures shown as small insets.

(B) Pair-wise distance distribution functions $P(r)$ calculated from SAXS data shown in Figures 3C and S3A for indicated constructs.

(C) Overall views of the asymmetric unit of the USP25 crystal structure. Residues are shown as lines and in cartoon representation. The overlaid electron density map in grey corresponds to weighted $2|F_o|-|F_c|$ electron density contoured at 1σ .

(D) Superposition of chain A on top of chain B forming one asymmetric unit. A superposition of symmetry-related chains C (corresponding to A) and D (corresponding to B) is also shown.

(E) Close-up view of the indicated dimerization interface of USP25 chains C and D (compare to Figure 2B on the right for the respective USP28 interaction). Relevant residues are shown as sticks. Residues mutated to generate monomeric USP25 are labeled in bold, residues characteristically different from the respective USP28 interface are labeled in italics.

(F) Sequence alignment of representative USP25 members of vertebrate families for the insertion sequence. Secondary structure and disorder assignments were carried out with respect to the USP25 catalytic domain structure.

(G) Sequence conservation calculated from USP25 protein sequences mapped as colored surface on chain A of the USP25 (157-714) structure in two orientations. Chains B, C and D are shown as semi-transparent cartoons.

(H) Superpositions of cartoon representations of the crystal structures of USP25 and USP28. Shown are an alignment of dimeric forms (*left*) and individual catalytic domains (*right*).

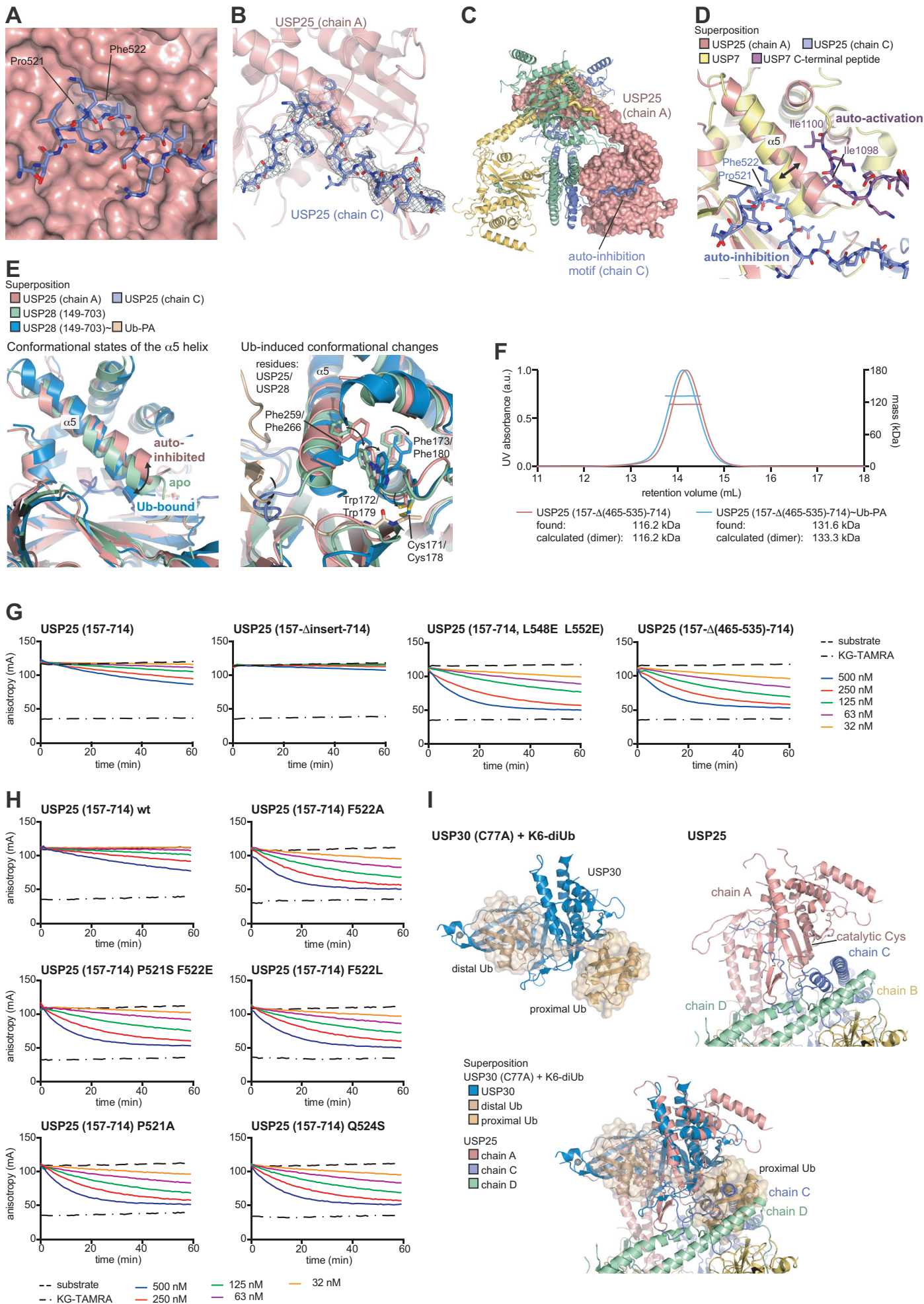


Figure S4. Mechanism of conserved auto-inhibition through oligomerization in USP25. Related to Figure 4.

(A) Close-up view of the pocket within the catalytic domain of USP25 (shown as red surface) that engages the auto-inhibition motif (shown as blue sticks).

(B) Electron density map in grey of the autoinhibition-motif contoured at 0.8σ corresponding to weighted $2|F_o| - |F_c|$ electron density. The USP25 catalytic domain is shown as a semitransparent cartoon.

(C) Cartoon representation of tetrameric USP25 as in Figure 3D. Chain A is shown as a surface to highlight binding of the AIM of chain C to the catalytic domain of chain A.

(D) Superposition of cartoon representations of USP25 (red) and USP7 (yellow, PDB-ID: 5JTJ) in complex with the auto-inhibition motif (blue) and the USP7 C-terminal activating peptide (purple), respectively. Their binding to opposite sites of the $\alpha 5$ helices of the catalytic domains and the diverging $\alpha 5$ conformations are highlighted by a black arrow. Key hydrophobic residues in both peptidic motifs are labeled.

(E) Superposition of indicated crystal structures in cartoon representation showing the different positioning of the $\alpha 5$ helix in the catalytic USP domains depending on auto-inhibition or ubiquitin binding (*left*). A putative conformational relay mechanism links the positioning of the $\alpha 5$ helix through the sidechain conformation of Phe259 (USP25) / Phe266 (USP28) to the catalytic cysteine and its following aromatic residues (*right*). Conformational changes are highlighted with black arrows. The cartoon representation of ubiquitin is not shown in the left panel for clarity.

(F) SEC-MALS analysis of USP25 constructs in which the sequence corresponding to the part that is disordered in USP28 is deleted (construct corresponds to USP28 (149- Δ (459-528)-703), see Figure S2F).

(G and H) Representative fluorescence anisotropy-time traces of Ub-KG-TAMRA cleavage assays of indicated USP25 proteins and concentrations. Catalytic efficiencies are shown in Figure 4D and 4F.

(I) Cartoon representation of inactive USP30 bound to K6-linked diubiquitin (PDB-ID: 5OHP), with distal and proximal ubiquitin moieties labeled and also shown as transparent surfaces (*top left*). Cartoon representation of USP25 (157-714) (*top right*). Superposition of both structures on the USP domain of chain A of USP25,

showing the clashing of the proximal ubiquitin moiety in its putative position with chains C and D from the second USP25 dimer (*bottom*).

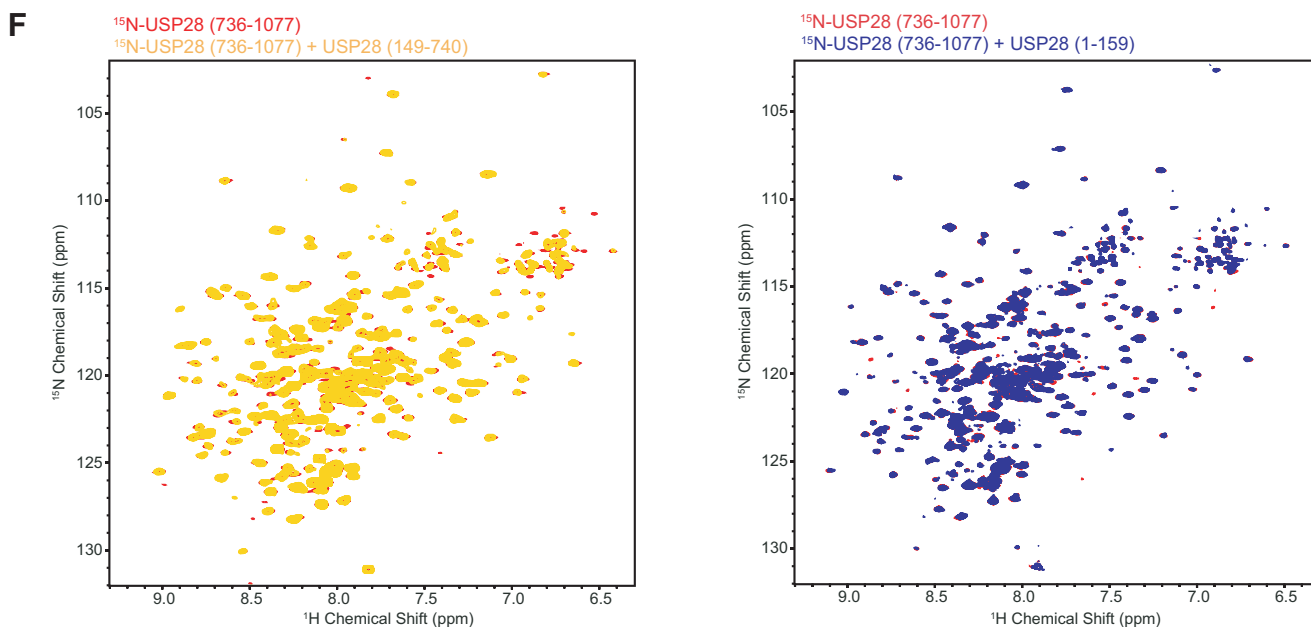
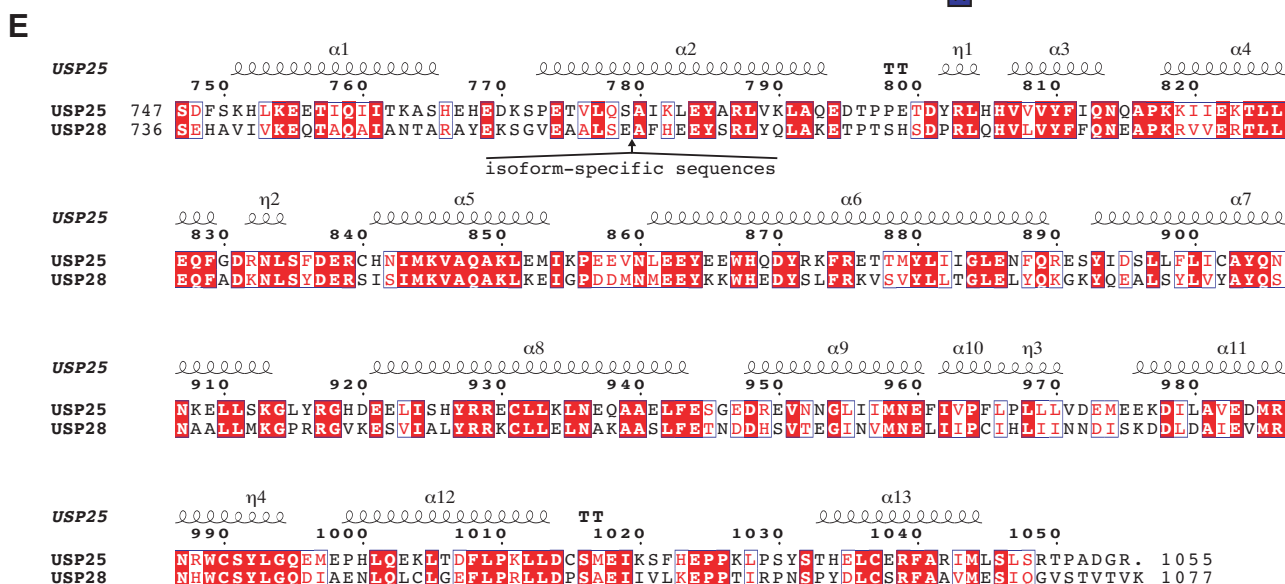
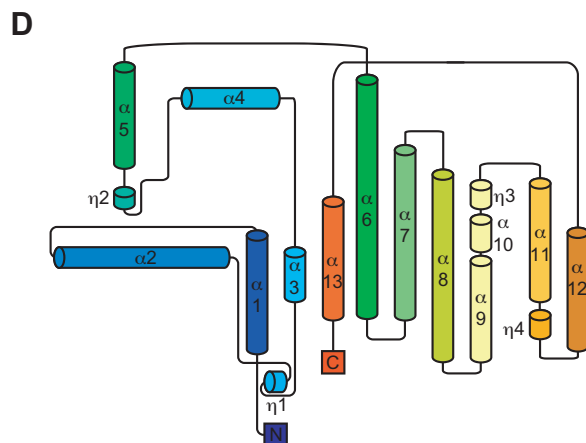
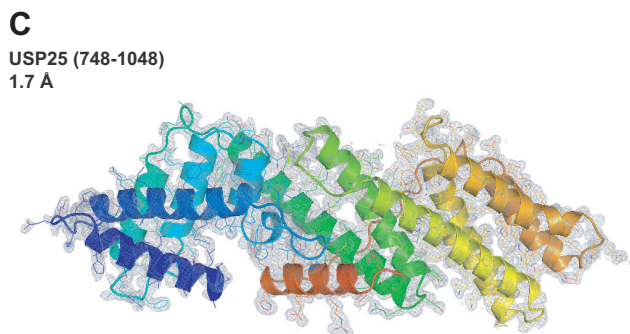
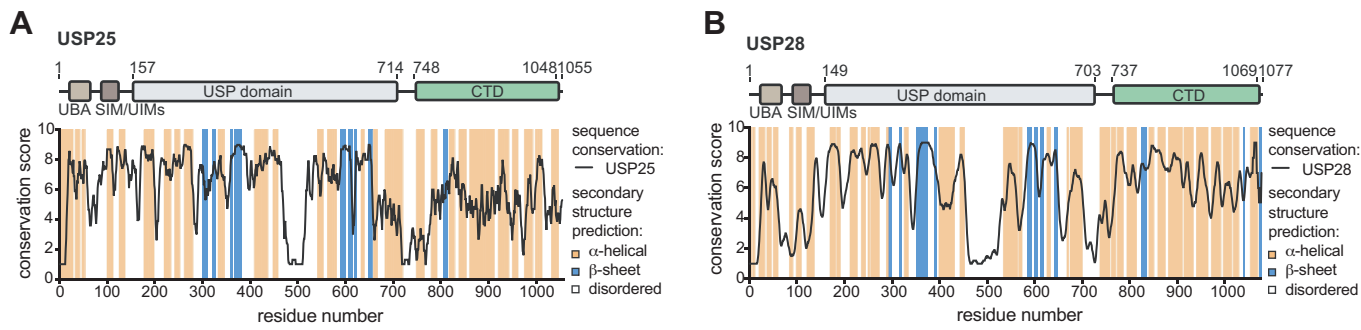


Figure S5. Structural analysis of the C-terminal domains of USP25 and USP28.

Related to Figure 5.

(A) Sequence conservation of USP25 plotted as a rolling window average in black of scores obtained from the ConSurf webserver. Secondary structure prediction of human USP25 from the Concord webserver indicated as background color. Schematic representation of the domain architecture of USP25 above the graph including the newly identified C-terminal domain.

(B) Analysis as in (A) for USP28.

(C) Overall view of the asymmetric unit of the crystal structures of USP25 (748-1048). Residues are shown as lines and in cartoon representation. The overlaid electron density map in grey corresponds to weighted $2|F_o|-|F_c|$ electron density contoured at 1σ .

(D) Topology diagram of the USP25 (748-1048) structure generated with the Pro-origami webserver. α helices and 3_{10} helices (η) are consecutively numbered.

(E) Sequence alignment of the C-terminal regions of human USP25 and USP28 with secondary structure elements indicated according to the USP25 (748-1048) structure. The insertion point where sequences of varying length are added to both USP25 and USP28 in isoforms lies within $\alpha 2$ of the CUEL domain. These sequences at least for USP25 customize the function of the DUB by facilitating different protein-protein interactions (Bosch-Comas et al., 2006). With large parts of the inserted sequences being predicted to be disordered, it is unknown how these would structurally remodel the C-terminal region of USP25 and USP28.

(F) ^1H - ^{15}N BEST-TROSY NMR spectra showing the ^{15}N -labeled C-terminal domain of USP28 (736-1077) (red) overlaid with ^{15}N -labeled USP28 (736-1077) in the presence of unlabeled USP28 (149-740) (yellow, *left*) or unlabeled USP28 (1-159) (blue, *right*). Labeled proteins were at $75 \mu\text{M}$ and unlabeled proteins were added to equimolar amounts.

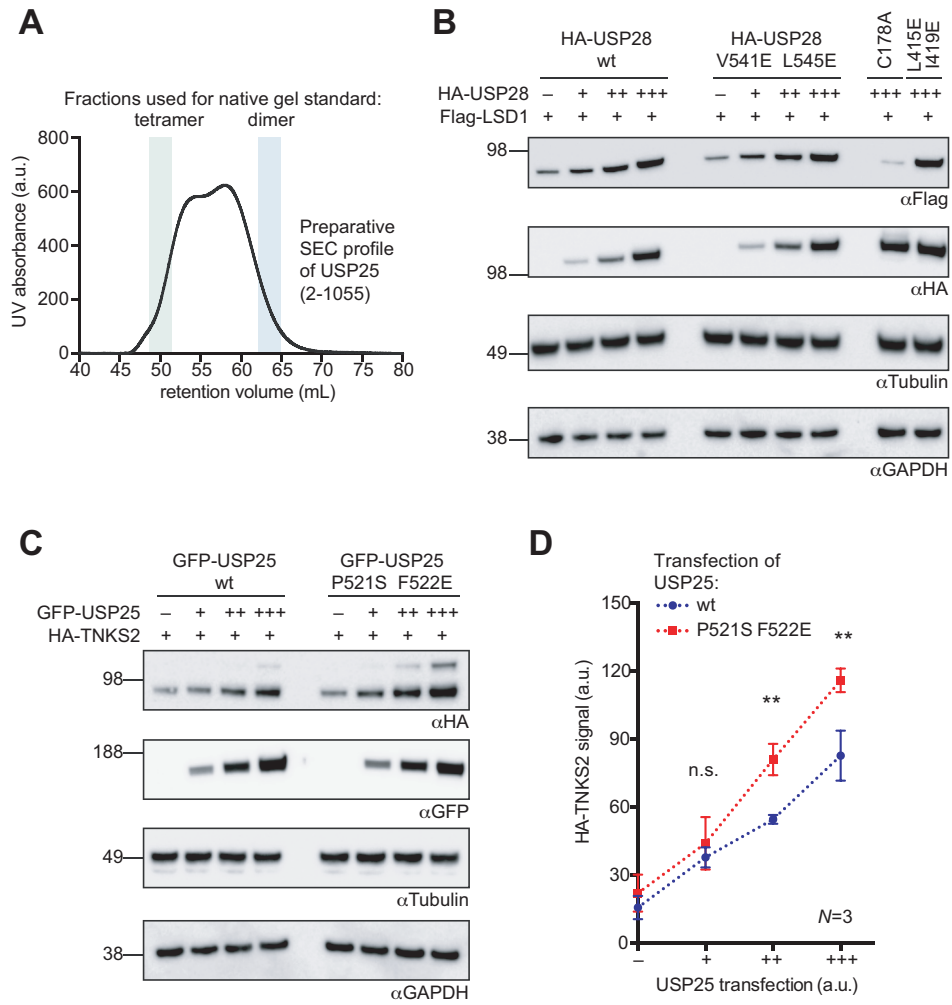


Figure S6. Functional assessment of oligomerization states of USP25 and USP28. Related to Figure 6.

(A) Size-exclusion chromatogram of full-length human USP25. Fractions used as size standards for native PAGE analysis are indicated with colors.

(B) Immunoblotting for indicated epitopes in lysates from HEK-293 cells transfected with vectors for the expression of Flag-LSD1 and increasing amounts of vector for HA-tagged USP28 proteins.

(C) Experiment as in B with HA-TNKS2 as substrate and increasing amounts of vector of GFP-tagged USP25 constructs. Since transfection of identical vector amounts of USP25 (P521S F522E) and USP25 wt led to a larger amount of protein of USP25 (P521S F522E), presumably due to its higher activity and increased auto-deubiquitination, the amounts of transfected vector were adjusted to achieve similar cellular protein concentrations.

(D) Quantification of the HA-TNKS2 immunoblotting signal from three independent repeats of the experiment shown in C. Data are shown as mean \pm standard deviation (**: $p < 0.01$, two-tailed t -test; n.s., not significant).

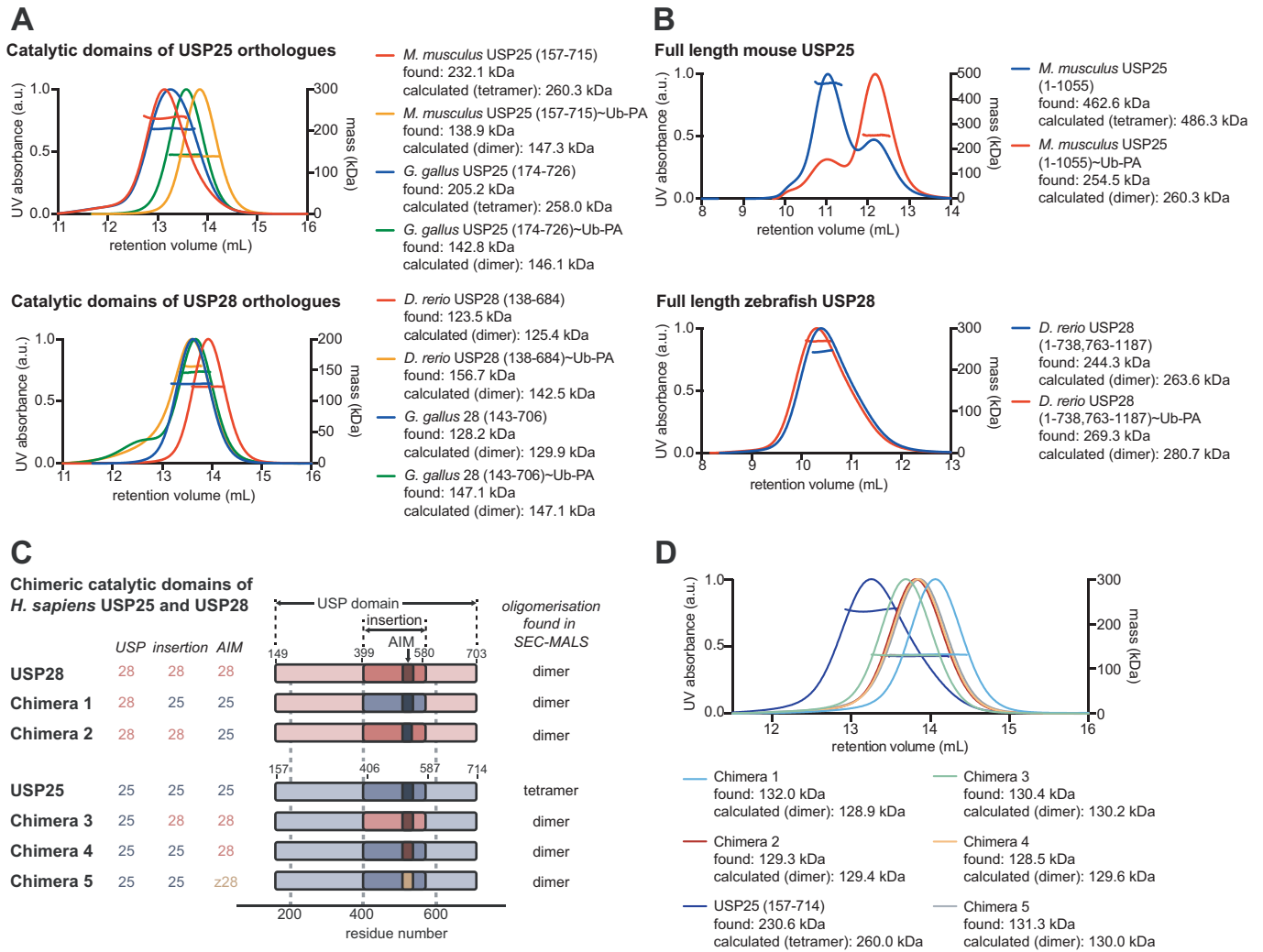


Figure S7. Molecular requirements for distinct oligomerization states of USP28 and USP25 catalytic domains. Related to Figure 7.

(A) SEC-MALS analysis of catalytic domains of USP28 orthologues (*top*) and catalytic domains of USP25 orthologues (*bottom*) both in their apo form and bound to Ub-PA. Identified masses are matched to either tetrameric or dimeric expected masses.

(B) SEC-MALS analysis of full length mouse USP25 (*top*) and full-length zebrafish USP28 (*bottom*) both in their apo form and bound to Ub-PA. Identified masses are matched to either tetrameric or dimeric expected masses.

(C) Schematic representation of chimeric catalytic domain constructs of human USP25 and USP28 proteins. Grafting of sequences was performed as indicated, based on equivalent positions identified from a sequence alignment and from superposition of structures (insertion of USP28: Y399-R580, “AIM”-equivalent sequence: S508-Q527; insertion of USP25: H406-I587, AIM: 515-534). In chimera 5, the AIM of human USP25 was replaced with the equivalent sequence of *D. rerio* USP28. The zebrafish USP28 sequence shares the central IHKPFTQ motif with the AIM of human USP25 (see Figure 4B), but contains different amino acids flanking this motif on both sides. These changes are sufficient to prevent tetramerization (see SEC-MALS data in B and D).

(D) SEC-MALS analysis of chimeric catalytic domain constructs shown in C and tetrameric USP25 as control. Identified masses are matched to either tetrameric or dimeric expected masses. Observed oligomerization states are listed in C.

Figure 1B
and 3B

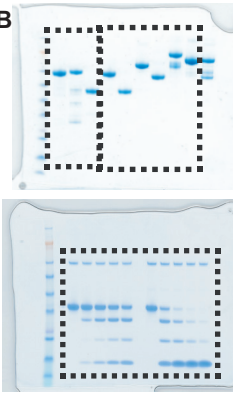


Figure 6A

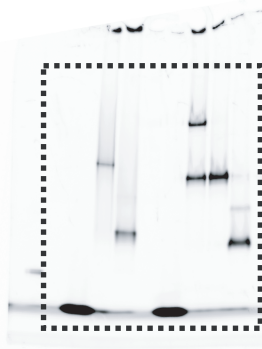


Figure 6B

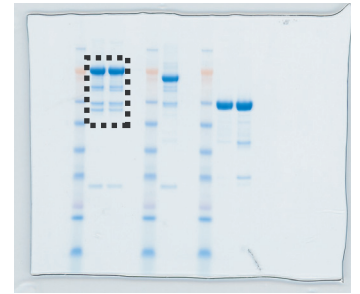
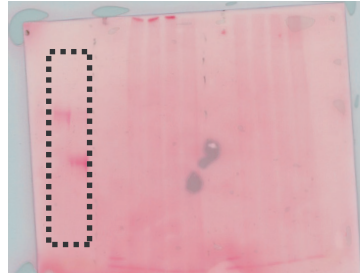


Figure 4G

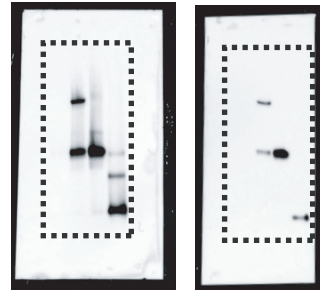
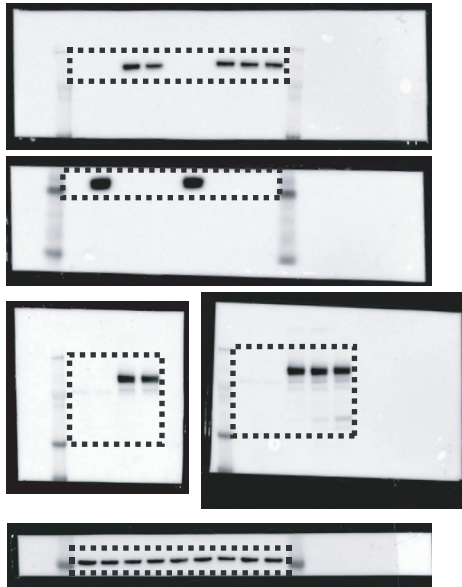
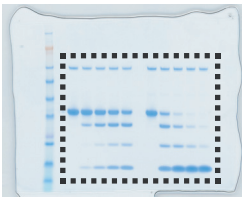


Figure 6C

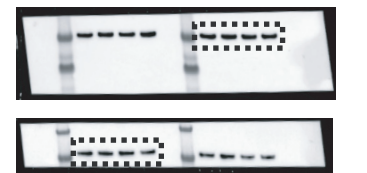
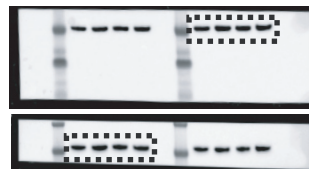
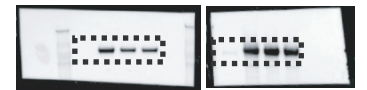
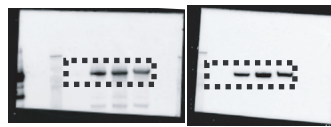
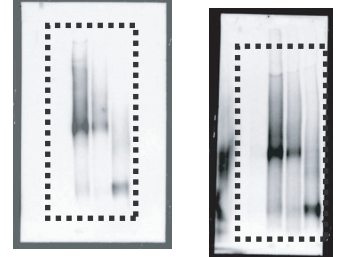
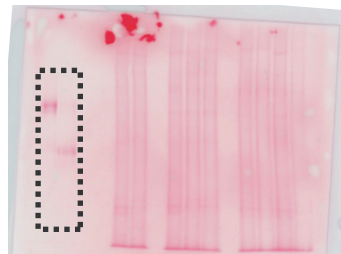
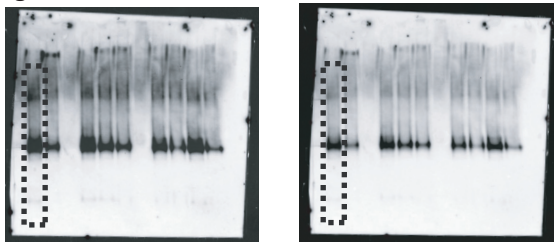


Figure 6D



Overlay

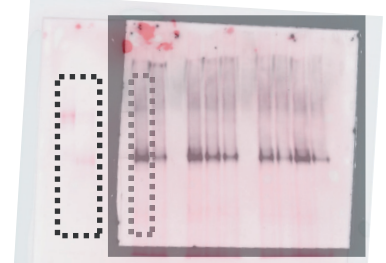


Figure 6E

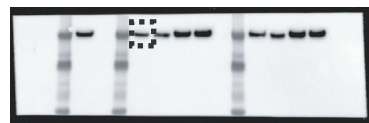
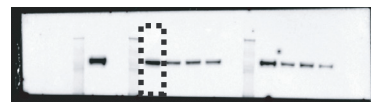
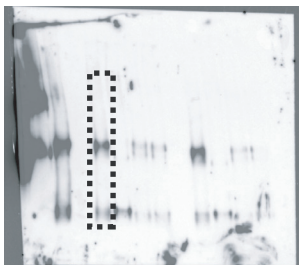


Figure S6B



Figure S6C



Figure S8. Uncropped gels and blots. Related to Figures 1, 3, 4, 6 and S6.

Supplemental Table 1. Parameters derived from SAXS data analysis. R_g denotes the radius of gyration obtained from Guinier plot fitting, D_{max} and R_{ave} denote the maximum distance and the average radius, respectively, obtained from real space data analysis. Related to Figures 2A, 3C and S3A.

Sample	R_g (Å)	D_{max} (Å)	R_{ave} (Å)	Peaks in $P(r)$ (Å)
USP28 149 -703 apo	50.6	145	65.1	33.8, 79.0
USP28 149-703~Ub-PA	51.4	146	64.3	35.3, 76.6
USP28 149- Δ insert-703 apo	24.1	73	30.9	30.8
USP28 149- Δ insert-703~Ub-PA	24.1	73	31.5	30.8
USP25 157-720 apo	45.8	130	60.5	61.8
USP25 157-720~Ub-PA	46.6	138	60.3	34.0, 73.8
USP25 157- Δ insert-720 apo	24.2	73	31.0	30.0
USP25 157- Δ insert-720~Ub-PA	24.9	73	31.8	30.4